S. Afr. J. Chem., 2026, 80, S293–S303
https://journals.co.za/content/journal/chem/

Green Chemistry-Driven Optimization of High-Performance Copper Corrosion Inhibition by *Ferula communis* L. (Apiaceae) Seed Essential Oil: Response Surface Methodology and Thermodynamic Insights

Ikram Djamai[1], Yazid Datoussaid[2,3]*, Chaouki Selles[1], Abbes Benchadli[4], Manal El Ali Ater[5], Alain Muselli[6], Sofiane Amara[7], and Tarik Attar[2,4]

[1]*Laboratory of Natural and Bioactive Substances (LASNABIO), Department of Biology, Tlemcen University, Imama, Tlemcen, Algeria.*
[2]*Ecole Supérieure en Sciences Appliquées de Tlemcen (ESSAT), Tlemcen, Algeria.*
[3]*Laboratory of Catalysis and Organic Synthesis (LCSCO), Faculty of Sciences, University of Tlemcen, Tlemcen, Algeria.*
[4]*Laboratory of Toxicomed, University Abou Beker Belkaid Tlemcen, Tlemcen, Algeria.*
[5]*Aix Marseille Univ, CNRS, Centre Interdisciplinaire de Nanoscience de Marseille, UMR 7325, Marseille, France.*
[6]*Université de Corse, UMR CNRS 6134, Laboratoire Chimie des Produits Naturels, BP 52, Corte, France.*
[7]*Materials and Renewable Energy Research Unit (URMER), University of Tlemcen, Tlemcen, Algeria.*

ABSTRACT

The growing need for sustainable corrosion mitigation has stimulated interest in plant-derived inhibitors as alternatives to conventional hazardous compounds. This study evaluates *Ferula communis* L. seed essential oil as a corrosion inhibitor for copper in 0.5 M H_2SO_4 using an integrated Response Surface Methodology (RSM) and thermodynamic approach. A 17-run Box–Behnken design was employed to examine the effects of inhibitor concentration (1–5%, v/v), temperature (293–333 K), and immersion time (0.5–1.5 hours), including their interactions. The resulting quadratic model exhibited high predictive capability (R^2 = 0.996, Q^2 = 0.978, RSD = 1.69%), with a model-predicted optimum inhibition efficiency of approximately 92.0%. The highest experimental efficiency within the design was 88.36%. SEM examination showed substantially reduced surface deterioration in the presence of the essential oil. Adsorption was best described by the Langmuir model, while thermodynamic analysis indicated a spontaneous and endothermic process with a predominantly physical contribution. Possible specific interactions between electron-rich inhibitor functionalities and copper surface sites may further influence interfacial stabilization. Overall, these findings demonstrate the potential of *F. communis* seed oil as a plant-derived corrosion inhibitor and highlight RSM as a useful approach for optimizing copper protection in acidic environments.

KEYWORDS

green corrosion inhibitor, *Ferula communis* essential oil, copper corrosion, response surface methodology (RSM), scanning electron microscopy (SEM).

Received: 21 July 2026 Revised: 3 September 2026 Accepted: 27 September 2026

INTRODUCTION

Copper stands among the most strategically valuable engineering metals, underpinning critical infrastructure across electronics, power transmission, thermal management, marine engineering, and petrochemical processing. Its unrivalled combination of electrical conductivity, thermal efficiency, mechanical ductility, and relative chemical stability has rendered it structurally irreplaceable in applications ranging from microelectronic circuitry and heat exchangers to desalination units and industrial pipelines.[1,2] Beyond energy applications, copper and its alloys are extensively used in condenser tubing, piping networks, electrical wiring, and chemical reactors, where efficient heat and charge transport are critical for system performance. Yet this same industrial ubiquity exposes copper components to a recurrent operational hazard: periodic immersion in strong acidic solutions during essential maintenance procedures such as descaling, acid pickling, chemical cleaning, and surface conditioning.[3] These processes are thermodynamically necessary to restore metallic surfaces by dissolving adherent oxide layers and inorganic deposits, but they simultaneously subject the underlying copper substrate to uncontrolled anodic dissolution a consequence of the metal's inability to sustain a stable protective passive film under highly acidic conditions.[4] Sulfuric acid occupies a dominant position in this context, constituting the most widely deployed industrial acid globally by virtue of its low cost, broad availability, and exceptional oxide-dissolving capacity. Its interaction with copper, however, is inherently destructive: in the absence of passivation, the metal dissolves progressively through sequential oxidation from Cu^0 to Cu^{2+}, generating surface damage, dimensional loss, and ultimately premature component failure.[5] The global cost of metallic corrosion has been estimated at approximately US$2.5 trillion annually, equivalent to roughly 3.4% of the world's gross domestic product with copper-intensive sectors bearing a disproportionate share of these losses through accelerated equipment replacement, unplanned operational shutdown, and material waste.[6] Identifying strategies capable of decoupling the necessary chemical aggressiveness of pickling baths from their destructive impact on copper surfaces therefore addresses a challenge of both scientific depth and immediate industrial relevance.

Corrosion inhibition represents the most operationally practical and cost-effective protective strategy in this context, requiring neither modification of process chemistry nor structural redesign of existing equipment.[7] Inhibitor molecules function by spontaneously adsorbing at the metal–electrolyte interface, forming a molecular barrier that reduces the active surface area accessible to corrosive ionic species and impedes both anodic dissolution and cathodic hydrogen evolution. The nature and strength of this interfacial interaction determine inhibitor durability. Physisorption occurs through electrostatic interactions between charged inhibitor species and the metal surface, whereas chemisorption proceeds through charge transfer or sharing between adsorbed inhibitor molecules and metal surface orbitals. Depending on the physicochemical characteristics of both the

*To whom correspondence should be addressed
Email: datouyazid@gmail.com

ISSN 1996-840X Online / South African Chemical Institute / http://saci.co.za/journal
© The Author(s) Published under a Creative Commons Attribution 4.0 International Licence (CC BY 4.0)
https://doi.org/10.17159/0379-4350/2026/v80se1a31

inhibitor and the metal surface, adsorption may be predominantly governed by physisorption, while localized donor–acceptor interactions contribute to stabilizing the adsorbed protective layer.[8] Thermodynamic parameters, including Gibbs free energy, enthalpy, and entropy changes, provide fundamental insight into adsorption spontaneity, thermal effects, and molecular reorganization at the metal/electrolyte interface.[9] Increasing environmental concerns and stricter regulatory requirements have accelerated the transition from conventional synthetic corrosion inhibitors toward sustainable plant-derived alternatives exhibiting lower toxicity, higher biodegradability, and abundant natural availability.[10] Plant extracts (phytochemicals) are being extensively utilized as green, effective, economically viable, and eco-friendly alternatives to traditional toxic corrosion inhibitors. Essential oils and phytochemical extracts constitute particularly compelling candidates, as they harbor structurally diverse families of bioactive molecules terpenes, phenolics, flavonoids, and oxygenated heterocycles whose multiple heteroatom centers and extended aromatic frameworks provide precisely the electronic architecture required for effective metal surface binding.[11] Recent investigations have confirmed the potential of plant-derived essential oils as sustainable and eco-friendly inhibitors in sulfuric acid media, achieving inhibition efficiencies exceeding 90% while exhibiting mixed-type inhibition behaviour consistent with Langmuir monolayer adsorption. Among relevant Mediterranean and North African species, *Ferula communis* L. (Apiaceae) is a spontaneous perennial plant widely distributed in the Mediterranean and Central Asian regions. It abundantly produces seeds whose size and weight vary according to ecological conditions. These seeds, elongated and cylindrical (3–6 mm), of dark brown to black colour, frequently present an integumentary dormancy requiring scarification or stratification treatments to improve their germination.[12] Furthermore, *F. communis* is recognized as a medicinal plant of interest, the species of the genus Ferula being rich in secondary biologically active metabolites. Their extracts are traditionally used in human and veterinary medicine for the treatment of various ailments, including digestive disorders, headaches, rheumatism, arthritis and certain tumoral pathologies, which highlights their important pharmacological potential.[13,14] Translating this protective potential into industrially actionable performance demands rigorous multi-variable optimization. The inhibition efficiency of any plant-derived system is governed not by concentration alone but by the simultaneous interplay of temperature, exposure duration, and inhibitor loading variables whose combined effects are nonlinear and mutually interactive.[15] Response Surface Methodology (RSM), coupled with an appropriate experimental design, provides an ideally suited statistical framework for this purpose: by fitting a second-order polynomial to a minimal, uniformly distributed set of experimental runs, it captures linear, quadratic, and interaction effects simultaneously, identifies interior optima within the design space, and delivers a validated predictive model with maximum information yield per experiment.[16, 17]

Accordingly, this study integrates response surface methodology, adsorption isotherm modeling, and thermodynamic analysis to comprehensively elucidate the corrosion inhibition performance of *Ferula communis* L. seed essential oil on copper in 0.5 M H_2SO_4, while identifying the optimum operating conditions and revealing the fundamental adsorption mechanism responsible for interfacial protection.

MATERIALS AND METHODS

Preparation of inhibitors

Ferula communis L. seeds were harvested in May 2025 from the Ourit area (34.882137° N, 1.2680884° W; 811.90 m above sea level), situated approximately 7 km from Tlemcen in north-western Algeria. Following collection, the seeds were air-dried and hydrodistilled using a Clevenger-type apparatus in accordance with the European Pharmacopoeia protocol.[18] Briefly, 400 g of dried seed material was distilled with 4 L of distilled water for 4 hours to obtain the essential oil. After extraction, the oil was transferred into airtight amber glass vials and preserved at 4 °C until further physicochemical characterization and corrosion inhibition experiments.

Chemical composition of essential oil

The chemical composition of the essential oil was characterized by gas chromatography equipped with flame ionization detection (GC–FID) and hyphenated gas chromatography–mass spectrometry (GC–MS) using a PerkinElmer Clarus 600 chromatograph and a PerkinElmer SQ8 TurboMass mass spectrometer, respectively. Separations were performed on two fused-silica capillary columns of complementary polarity, namely Rtx-1 (polydimethylsiloxane) and Rtx-Wax (polyethylene glycol) (60 m × 0.22 mm i.d., 0.25 μm film thickness). The oven temperature was programmed from 60 to 230 °C at a heating rate of 2 °C min^{-1} and maintained at the final temperature for 30 min. Both the injector and detector were operated at 280 °C, while hydrogen served as the carrier gas at a constant flow rate of 0.7 mL min^{-1}. Samples were injected in split mode (1:80), using injection volumes of 0.2 μL for GC–FID and 0.1 μL for GC–MS analyses. Retention indices (RI) were determined relative to a homologous series of *n*-alkanes (C_5–C_{30}) following the method of Van den Dool and Kratz. Mass spectra were acquired under electron ionization (70 eV), with the ion source maintained at 150 °C over a mass range of 35–350 *m/z*. Compound identification was achieved through combined comparison of retention indices and mass spectral data with reference databases and published literature.[19]

Weight-loss measurements

Copper coupons of high purity and rectangular geometry were used for the gravimetric measurements. Before each experiment, the specimens were mechanically polished using SiC abrasive papers with progressively finer grades (600, 800, 1000, and 1200 grit). The surfaces were subsequently rinsed with double-distilled water, degreased with acetone, and dried using a stream of warm air. The initial mass of each coupon was determined immediately before exposure with an analytical balance having a resolution of ±0.1 mg. The test electrolyte was prepared from analytical-grade 98% H_2SO_4 and double-distilled water to obtain a final concentration of 0.5 M. The inhibitor media were prepared by directly dispersing the required amount of essential oil in the acidic solution to give concentrations ranging from 1 to 5% (v/v). No co-solvent or emulsifying agent was introduced. The resulting preparations were visually examined to ensure that no macroscopic phase separation occurred during the exposure period. The corrosion tests were carried out under static conditions in a thermostatically controlled water bath. The temperature was varied between 293 and 333 K, with a stability of ±1 K, while the immersion period was set between 0.5 and 1.5 hours. At the end of each exposure, the coupons were removed from the solution, thoroughly rinsed, dried, and weighed using the same analytical procedure. The mass-loss data were subsequently used to calculate the corrosion rate and inhibition efficiency according to the established gravimetric equations.[20,21] All experiments were conducted in triplicate, and the reported values correspond to the mean ± standard deviation of the three independent measurements.

Adsorption and Thermodynamic Investigations

The interaction between the plant-derived inhibitor and the copper surface in 0.5 M H_2SO_4 was thermodynamically characterized using weightloss data collected from 293 to 333 K. Surface coverage fractions (θ) were calculated from inhibition efficiencies and then fitted to four classical isotherms (Langmuir, Freundlich, Frumkin, and Flory–Huggins) following standard protocols.[22,23] The most appropriate model was selected based on regression quality, and the corresponding adsorption equilibrium constant (K_{ads}) was extracted.

From K_{ads}, the Gibbs free energy change of adsorption (ΔG_{ads}) was derived using the accepted relationship that incorporates the solvent molar concentration. A linear plot of ΔG_{ads} versus temperature subsequently provided the adsorption enthalpy (ΔH_{ads}) and entropy (ΔS_{ads}) via the Gibbs–Helmholtz formalism.[24] These quantities reveal the spontaneity, exothermic/endothermic nature, and ordering phenomena at the metal–electrolyte interface. Separately, the temperature dependence of corrosion rates (CR) was exploited to evaluate kinetic barriers. Applying the Arrhenius approach, the activation energy (E_{act}) was obtained from the slope of ln(CR) against reciprocal temperature. Transitionstate theory (Eyring) gave access to the activation enthalpy (ΔH_{act}) and entropy (ΔS_{act}) from the ln(CR/T) versus 1/T plot.[25] The activation free energy (ΔG_{act}) at 308 K was then computed by inserting ΔH_{act} and ΔS_{act} into the same thermodynamic relation used for adsorption.[26] Together, the adsorption and activation parameters offer complementary insights: the former quantify the inhibitor's surface affinity and layer stability, while the latter describe how the extract modifies the energy barrier for copper dissolution. This integrated thermodynamic framework, provides a robust mechanistic interpretation of corrosion protection under the tested conditions.

Scanning Electron Microscopy (SEM)

The morphology of the copper surface was characterized using a Hitachi TM1000 scanning electron microscope at 500× magnification (200 µm scale bar). Copper specimens were immersed for 1 hour in 0.5 M H_2SO_4 under the optimized conditions, either without or with *Ferula communis* L. seed essential oil. SEM images were acquired for the polished substrate and for the specimens after exposure to the corrosive medium. The resulting micrographs were used to evaluate corrosion-induced surface damage and the formation of the inhibitor-derived protective layer.

Design of experiments study

Response Surface Methodology (RSM)

Statistical optimization was conducted using Response Surface Methodology implemented in MODDE® 9.1 (Sartorius, Germany). The study considered three operational parameters, namely inhibitor concentration (X_1), temperature (X_2), and immersion time (X_3), arranged according to a central composite face-centered (CCF) design. Each factor was explored at three coded levels (−1, 0, and +1), yielding a set of 17 experiments that incorporated factorial, axial, and replicated center points. This configuration provided sufficient information to characterize response curvature while ensuring experimental consistency.[27] Inhibition efficiency (IE) served as the response variable and was described through a second-order polynomial expression containing linear, quadratic, and cross-product contributions. Estimation of the regression parameters was achieved by multiple linear regression (MLR), enabling quantification of both the direct influence of each factor and their mutual interactions. Statistical significance and predictive robustness were verified through analysis of variance (ANOVA) and several key diagnostic metrics: determination coefficient (R^2), adjusted R^2 (R^2 Adj.), predictive coefficient (Q^2), relative standard deviation (RSD), standard deviation of the response (SDY), condition number (Cond. no.), reproducibility, and model validity.[28,29] Response surface and contour representations were further generated to illustrate variations in IE throughout the investigated region. The resulting mathematical model provided a reliable basis for identifying the operating conditions associated with the highest inhibition performance and for clarifying the interdependence among the examined variables.[30]

RESULTS AND DISCUSSION

Chemical composition of essential oil

GC–MS analysis revealed that the essential oil extracted from Ferula communis L. seeds possesses a chemically diverse composition, with 69.0% of its constituents successfully characterized (Table 1). The oil was overwhelmingly dominated by hydrocarbon constituents (69.0%), of which monoterpene hydrocarbons constituted the principal fraction (67.1%), whereas sesquiterpene hydrocarbons accounted for only 1.9%. α-Pinene was the most abundant constituent (32.2%), followed by limonene (19.3%) and β-pinene (9.3%). Minor amounts of other monoterpene hydrocarbons, including myrcene (3.3%), sabinene (1.1%), β-phellandrene (1.1%), and γ-terpinene (0.7%), were also detected. The sesquiterpene hydrocarbon α-guaiene represented the sole member of this class, contributing 1.9% of the total composition.

Effect of the Acidic Medium

Before RSM optimization, the protective performance of *Ferula communis* seed essential oil was evaluated in four 1 N mineral acid media. The inhibition efficiency followed the sequence H_2SO_4 (85.77%) > $HClO_4$ (77.53%) > HCl (68.15%) > HNO_3 (52.61%), indicating a pronounced dependence on the acidic medium. This behaviour cannot be attributed to a single factor, as several physicochemical characteristics of the electrolyte may simultaneously affect copper

Table 1: Chemical composition of *Ferula communis* seeds essential oil identified by GC-MS analysis.

N°[a]	Compound[a]	RI_a[c]	RI_a[d]	RI_p[e]	Essential oil[e] (%)[f]	Identification[g]
1	α-Pinene	931	938	1030	32.2	RI, MS
2	Sabinene	964	973	1122	1.1	RI, MS
3	ß-Pinene	970	978	1112	9.3	RI, MS
4	Myrcene	983	989	1159	3.3	RI, MS
5	ß-phelandrane	1020	1019	1208	1.1	RI, MS
6	Limonene	1020	1029	1199	19.3	RI, MS
7	γ-terpinene	1047	1057	1248	0.7	RI, MS
8	α-guaiene	1440	1430	1584	1.9	RI, MS
	Total identification %				69.0	

Family of compounds	
Hydrocarbon compounds	69.0
Monoterpene hydrocarbons	67.1
Sesquiterpene hydrocarbons	1.9

[a] compounds identified by GC-MS,[b-e] retention indices (RI) obtained experimentally and compared with literature data,[f] relative percentage (%) of each compound in the essential oil, [g] identification methods: RI :retention indices and MS :mass spectrometry (see experimental).

corrosion and inhibitor adsorption. Differences in acid strength, ionic conductivity, counter-anion characteristics, interfacial competition for copper surface sites, and the specific dissolution chemistry of copper may all contribute to the observed variation. Among these factors, the nature of the counter-anion deserves particular consideration. The comparatively high inhibition efficiency observed in H_2SO_4 may be partly attributed to the specific characteristics of the sulfate anion. Unlike chloride (Cl^-), which is known to form soluble complexes with copper ions and thereby accelerate dissolution, or nitrate (NO_3^-), which exhibits oxidizing properties that can interfere with the corrosion process, sulfate ions (SO_4^{2-}) are known to adsorb only weakly on copper surfaces and do not form soluble complexes that would promote metal dissolution. Furthermore, the divalent sulfate anion may facilitate the initial electrostatic attraction of protonated inhibitor species to the positively charged copper surface, thereby promoting subsequent adsorption of the organic constituents. In contrast, the relatively low inhibition efficiency in HNO_3 may also be associated with the oxidizing character of nitrate-containing acidic media, which can alter the copper surface state and compete with inhibitor adsorption. However, the present data do not allow a quantitative separation of the anion's contribution from other electrolyte-dependent effects, and the observed inhibition sequence should therefore be interpreted as the net result of multiple interacting factors. Differences in interfacial organization and possible interactions involving the counter-anions may likewise influence the accessibility of copper surface sites and the formation or persistence of the inhibitor-derived protective layer. Therefore, the observed inhibition sequence is considered to result from the combined effects of electrolyte-dependent corrosion kinetics, interfacial processes, and inhibitor–surface interactions rather than from a single controlling mechanism. Based on its comparatively high inhibition efficiency, 0.5 M H_2SO_4 was selected as the working electrolyte for the subsequent RSM optimization experiments.

Experimental Design and RSM Model Development

A response surface design comprising 17 experimental runs including three central-point replicates was employed to quantify the individual and combined effects of inhibitor concentration (X_1: 1–5%), temperature (X_2: 293–333 K), and immersion time (X_3: 0.5–1.5 hours) on the corrosion inhibition efficiency (IE%) of the essential oil against copper dissolution in 0.5 M H_2SO_4. The full experimental matrix and corresponding measured IE% values are presented in Table 2. The measured IE% spanned a wide dynamic range, from a minimum of 25.15% recorded at the lowest concentration, temperature, and exposure time (C = 1%, T = 293 K, t = 0.5 hour) to a maximum of 88.36% achieved at the highest concentration and intermediate conditions (C = 5%, T = 313 K, t = 1 hour). This substantial amplitude across the design space confirms the pronounced sensitivity of the protective response to variations in the operating parameters and validates the choice of the design for capturing both linear and nonlinear response behaviour.[31] Regression analysis of the experimental dataset yielded the following second-order polynomial model in coded variables:

$$IE\ (\%) = 68.166 + 17.120X_1 + 11.788X_2 + 0.795X_3 + 1.392X_1^2 - 3.228X_2^2 - 6.533X_3^2 - 4.201X_1X_2 - 0.169X_1X_3 - 0.331X_2X_3$$

where X_1, X_2 and X_3 denote the coded values of concentration, temperature, and immersion time, respectively.

The positive linear coefficients associated with concentration (+17.120) and temperature (+11.788) identify these two variables as the principal drivers of efficiency enhancement, while the negative quadratic terms for time (−6.533) and temperature (−3.228) reveal curvature and the existence of optimal operating values within the studied domain. The antagonistic interaction term Con×Temp (−4.201) further indicates that the combined effect of these two variables produces a response below their individual additive contributions, underscoring the necessity of simultaneous multi-variable optimization rather than univariate approaches.[32]

Statistical Validation and Model Adequacy

The statistical performance of the developed model is summarized in Table 3. The coefficient of determination $R^2 = 0.996$ indicates that 99.58% of the total variance in the inhibition efficiency response, confirming an exceptional level of agreement between experimental observations and predicted values. The adjusted coefficient $R^2_{adj} = 0.990$ remains in close proximity to R^2, demonstrating that the model retains its predictive power without evidence of overfitting introduced by the inclusion of non-significant terms. The cross-validated predictive coefficient $Q^2 = 0.978$ further substantiates the strong generalization capability of the model, as the narrow gap between R^2 and Q^2 ($\Delta R^2–Q^2 = 0.018$) falls well within the acceptable threshold of 0.2, beyond which overfitting is considered statistically significant.[32]

The model validity score of 0.914, exceeding the recommended threshold of 0.25, confirms the structural adequacy of the polynomial equation.[33] The reproducibility value of 0.987, derived from the three central-point replicates, attests to the excellent experimental precision and low measurement noise throughout the design. The condition number of 4.438 is well below the critical value of 10, confirming the numerical stability of the regression matrix and the absence of multicollinearity among the independent variables.

The residual standard deviation (RSD = 1.692%) is negligible relative to the IE% response amplitude. As detailed in Table 4, the maximum absolute deviation between observed and predicted values across all 17 runs is 2.22%, which remains below the largest 95% confidence interval halfwidth (3.57%) and is comparable to the narrowest interval (±1.71%).

Table 2. Experimental design matrix with observed inhibition efficiency (IE%) values for copper in 0.5 M H_2SO_4.

Exp No	Concentration (%, V/V)	Temperature (K)	Time (hours)	IE (%)
1	1	293	0.5	25.15
2	5	293	0.5	67.39
3	1	333	0.5	58.45
4	5	333	0.5	83.99
5	1	293	1.5	28.05
6	5	293	1.5	69.72
7	1	333	1.5	60.13
8	5	333	1.5	84.89
9	1	313	1	51.37
10	5	313	1	88.36
11	3	293	1	54.88
12	3	333	1	75.61
13	3	313	0.5	61.87
14	3	313	1.5	62.01
15	3	313	1	65.95
16	3	313	1	67.45
17	3	313	1	69.87

Table 3. RSM model adequacy statistics for the inhibition efficiency (IE%) response.

	R^2	Q^2	R^2 Adj.	RSD	SDY	Cond. no.	Reproducibility	Model Validity
IE	0.996	0.978	0.990	1.692	17.230	4.438	0.987	0.914

Table 4. Comparison of experimentally observed and model-predicted IE% values with residuals and 95% confidence intervals across all 17 runs.

IE	Observed	Predicted	Obs - Pred	Conf. int(±)
1	25.15	25.3937	-0.2437	3.5674
2	67.39	68.3737	-0.9837	3.5674
3	58.45	58.0347	0.4153	3.5674
4	83.99	84.2097	-0.2197	3.5674
5	28.05	27.9837	0.0663	3.5674
6	69.72	70.2887	-0.5687	3.5674
7	60.13	59.2997	0.8303	3.5674
8	84.89	84.7997	0.0903	3.5674
9	51.37	52.4382	-1.0682	2.8731
10	88.36	86.6782	1.6818	2.8731
11	54.88	53.1502	1.7298	2.8731
12	75.61	76.7262	-1.1162	2.8731
13	61.87	60.8382	1.0318	2.8731
14	62.01	62.4282	-0.4182	2.8731
15	65.95	68.1658	-2.2158	1.7123
16	67.45	68.1658	-0.7158	1.7123
17	69.87	68.1658	1.7042	1.7123

In addition, the parity plot (Figure 1a) shows excellent agreement, with all experimental points tightly scattered around the diagonal line. The normal probability distribution of studentized residuals (Figure 1b) reveals no significant outliers or systematic departures. Collectively, these results confirm full adherence to regression assumptions, with no evidence of systematic bias, heteroscedasticity, or outlier influence.[34]

Factor Analysis: Regression Coefficients, Effect Magnitudes, and Main Effects

The regression coefficients (Table 5), ranked effect magnitudes (Table 6), and the corresponding effect plot (Figure 2) provide mutually consistent quantification of the relative importance of the model terms. Inhibitor concentration carries both the largest linear coefficient (β_1 = +17.12, p = 7.54 × 10^{-9}) and the highest absolute standardised effect (34.24 ± 2.53%), unambiguously identifying it as the dominant variable governing corrosion protection. As illustrated in Figure 3a, the concentration response exhibits a quasilinear enhancement of IE% from ~52% at 1% to ~88% at 5%, with no saturation plateau, reinforcing the continuity and barrier effectiveness of the protective film against H^+ and SO_4^{2-} attack.[35]

Temperature ranks second in influence (β_2 = +11.79, p = 1.00 × 10^{-7}; effect = 23.58 ± 2.53%), its strong positive linear effect being thermodynamically consistent with an endothermic adsorption process. The main effects plot for temperature (Figure 3b) displays a

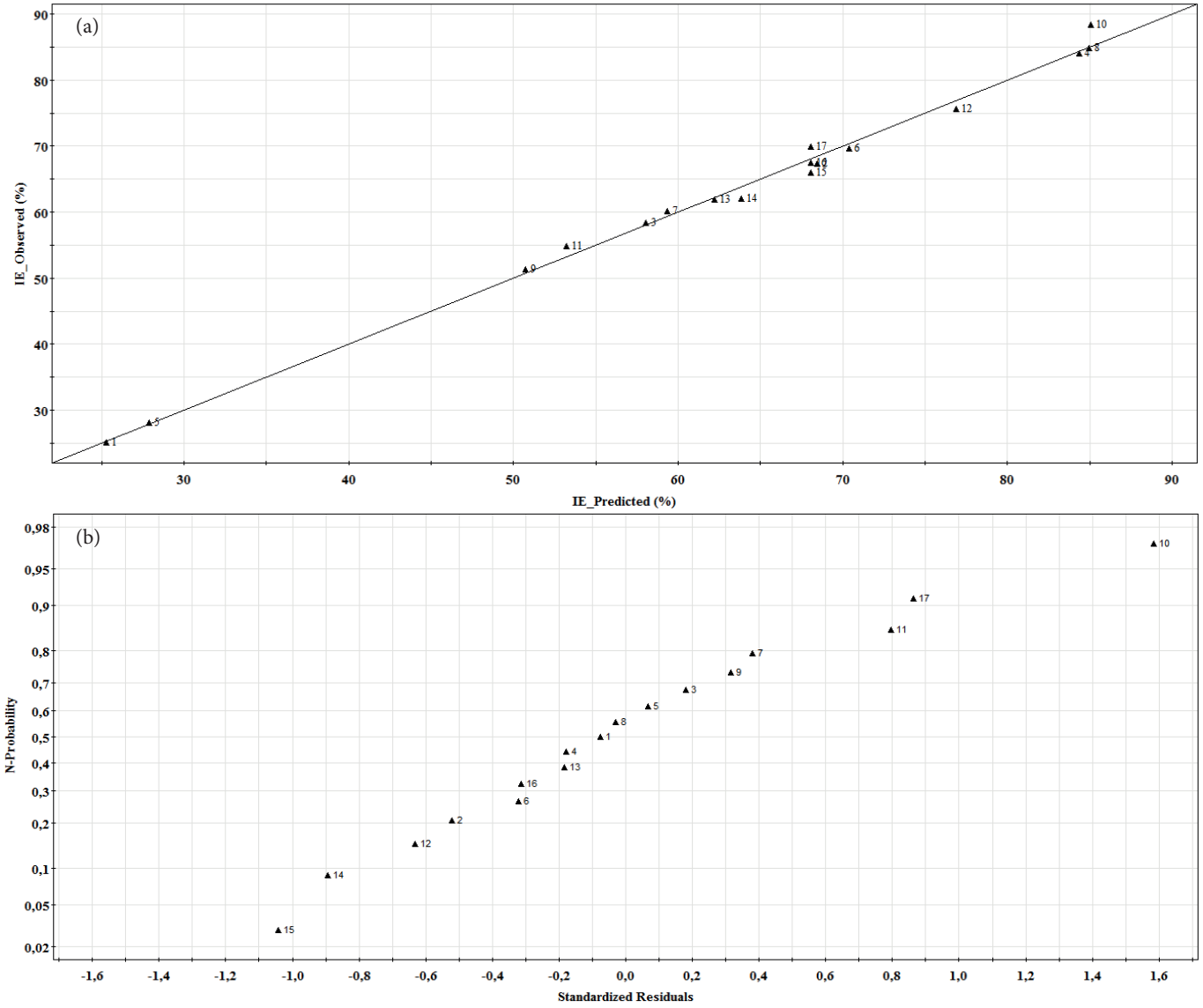


Figure 1: (a) Diagnostic plot comparing RSM model-predicted and experimentally measured inhibition efficiency values and (b) normal probability plot of residuals

Table 5. Standardised effects and confidence intervals ranked in descending order of absolute magnitude, with physical interpretation of each contribution.

IE	Coeff. SC	Std. Err.	P	Conf. int(±)
Constant	68.166	0.724	4.02×10^{-12}	1.712
X_1	+17.120	0.535	7.54×10^{-9}	1.265
X_2	+11.788	0.535	1.00×10^{-7}	1.265
X_3	+0.795	0.535	0.181	1.265
X_1^2	+1.392	1.034	0.220	2.445
X_2^2	−3.228	1.034	0.017	2.445
X_3^2	−6.533	1.034	3.97×10^{-4}	2.445
X_1X_2	−4.201	0.598	2.07×10^{-4}	1.415
X_1X_3	−0.169	0.598	0.786	1.415
X_2X_3	−0.331	0.598	0.597	1.415

Table 6. Estimated main, quadratic, and interaction effects with corresponding confidence intervals for the response surface model of inhibition efficiency (IE%).

Factor / Interaction	Effect (±)	Conf. Int. (±)
X_1	+34.24	2.531
X_2	+23.58	2.531
X_3^2	−13.07	4.890
X_1X_2	−8.40	2.830
X_2^2	−6.46	4.890
X_1^2	+2.78	4.890
X_3	+1.59	2.531
X_2X_3	−0.66	2.830
X_1X_3	−0.34	2.830

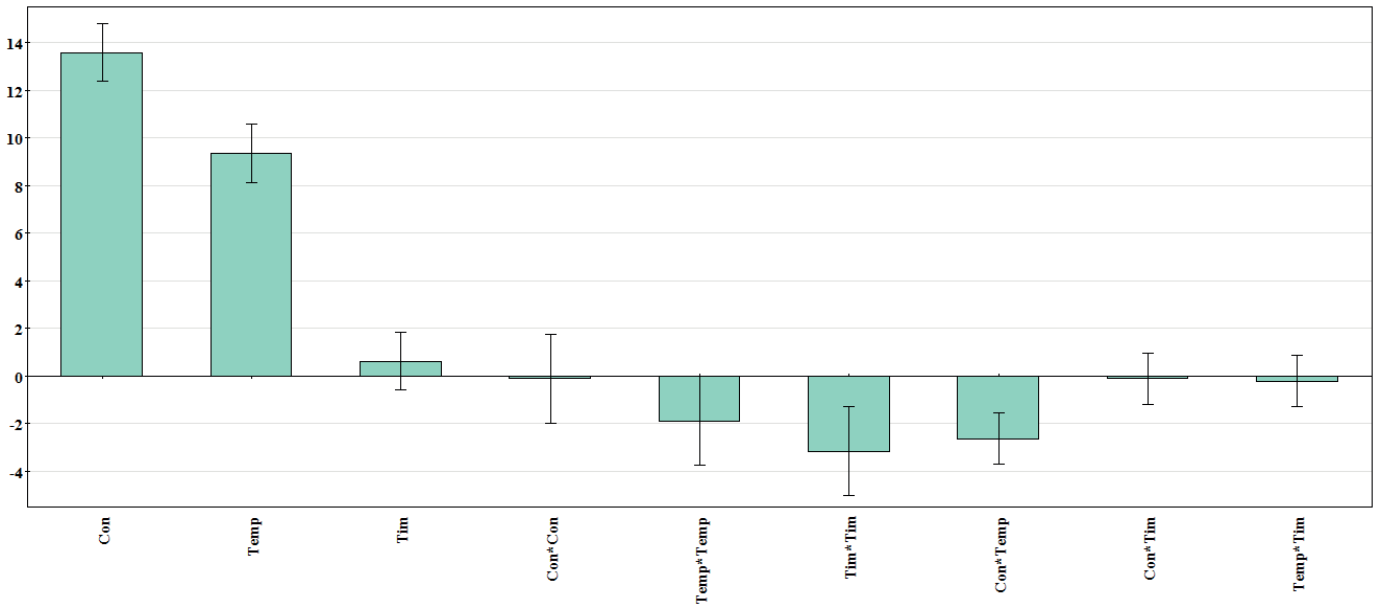


Figure 2: Standardised effects of factors and interactions (data from Table 5).

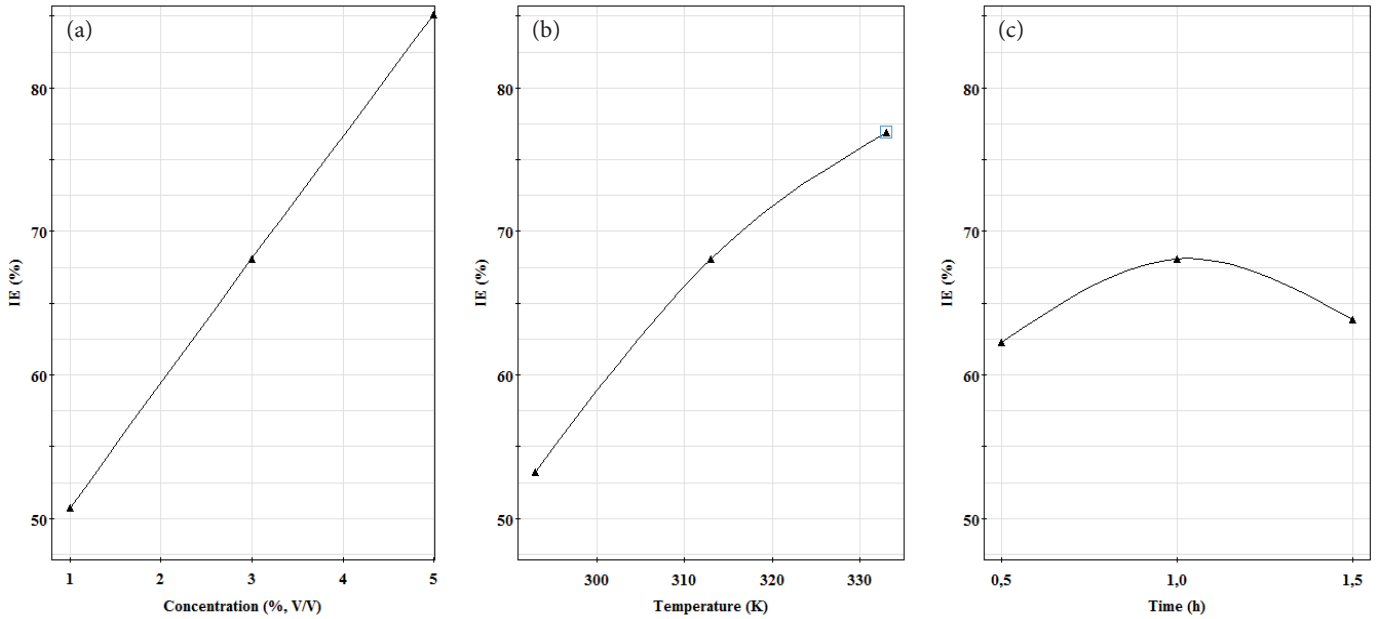


Figure 3: Main effect plots showing the influence of inhibitor concentration (a) temperature, (b) immersion time and (c) on the inhibition efficiency (IE%).

monotonically increasing yet concave profile: IE% rises from ~53% at 293 K to ~76% at 333 K with a diminishing rate, confirming approach toward surface coverage saturation. This thermally promoted behaviour reflects an endothermic adsorption process: rising thermal energy facilitates displacement of preorganized interfacial water and sulfate species, enabling stronger anchoring of phytochemical constituents onto the copper substrate, while the decelerating slope at higher temperatures signals nearsaturation.[36] The linear effect of immersion time (β_3 = +0.795, p = 0.181) is statistically nonsignificant at the 95% confidence level, indicating that contact duration alone exerts no direct steadystate influence within the studied range. The main effects curve for time (Figure 3c) correspondingly exhibits a parabolic profile: IE% peaks near t = 1 hour (~68%) before declining to ~62% at t = 1.5 hours. This bellshaped response is mathematically encoded by the dominant quadratic term t^2 ($\beta_{33} = -6.533$, $p = 3.97 \times 10^{-4}$; effect = −13.07 ± 4.89%), identifying a kinetically optimal contact window. As shown in Figure 3c, beyond this window, competitive desorption, acidinduced film thinning, or progressive ionic readsorption progressively undermines the structural cohesion of the protective layer.[37] Notably, the immersion time curve departs markedly from monotonicity, with the maximum near 1 hour followed by a gradual decline to ~62% at 1.5 hours. Among the remaining model terms, T^2 ($\beta_{22} = -3.228$, p = 0.017; effect = −6.46 ± 4.89%) confirms the concave saturation curvature of the temperature response, while C^2 (p = 0.220) is nonsignificant, indicating that concentration exerts a predominantly linear beneficial influence without selflimiting curvature within the studied range. The Con×Temp interaction ($\beta_{12} = -4.201$, $p = 2.07 \times 10^{-4}$; effect = −8.40 ± 2.83%) is the sole statistically significant crossterm, revealing an antagonistic coupling between the two dominant variables: at high surface coverage achieved by maximum loading, the incremental benefit of temperaturedriven interfacial water displacement diminishes, rendering these variables partially substitutable rather than fully additive. The Con×Tim and Temp×Tim interactions (p > 0.59) are nonsignificant, confirming that concentration and temperature operate independently of exposure duration.

Response Surface Analysis and Optimal Conditions

The two-dimensional contour plots and three-dimensional response surface (Figures 4 and 5) illustrate the combined influence of inhibitor concentration and temperature on IE% at fixed immersion time.[38] The surface topology reveals a pronounced ascending ridge oriented along the concentration axis, superimposed on a concave curvature in the temperature direction, generating a well-defined region of maximal efficiency at high concentration and intermediate-to-high temperature. The contour lines shift progressively toward higher IE% values as concentration increases, with the gradient steepest at low temperatures where the additional molecules compensate for reduced thermal activation. At the highest concentration (5%) and temperature (333 K), the response surface plateaus near 88–89%, signaling approach toward the physical saturation limit of the copper surface under the current experimental conditions. The contour analysis at varying immersion times further confirms that 1 hour (Figure 4b)represents the optimal exposure window, with plots generated at 0.5 hour (Figure 4a) and 1.5 hours (Figure 4c) yielding systematically lower predicted efficiencies across the entire concentration–temperature space, reinforcing the parabolic time dependence identified in the regression analysis.

The response surface model identified an optimum operating domain at approximately 5% inhibitor concentration, 333 K, and 1 hour immersion, corresponding to a predicted inhibition efficiency of about 92%. Experimental validation closely matched the model prediction, confirming the robustness and predictive accuracy of the developed quadratic equation. The pronounced concentration–temperature interaction observed within the response surface further demonstrates that maximizing corrosion protection requires multivariable optimization rather than independent variation of individual parameters, thereby providing a reliable framework for the rational development of sustainable corrosion-control systems.

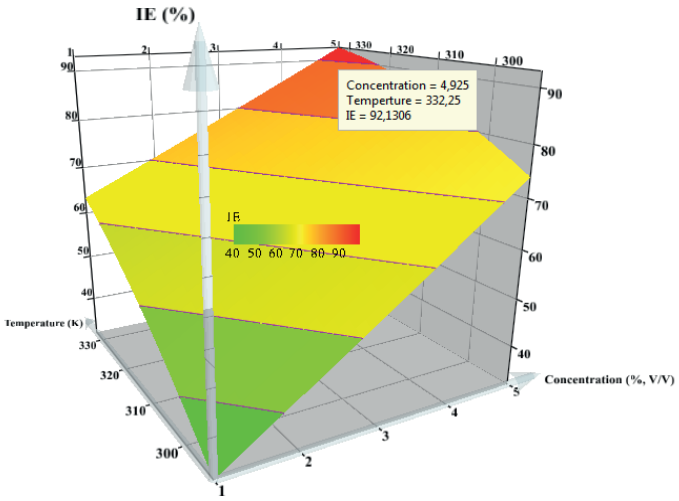


Figure 5: Three-dimensional response surface plot of inhibition efficiency (IE%) as a function of inhibitor concentration and temperature at the optimal immersion time (t = 1 hour) in 0.5 M H_2SO_4.

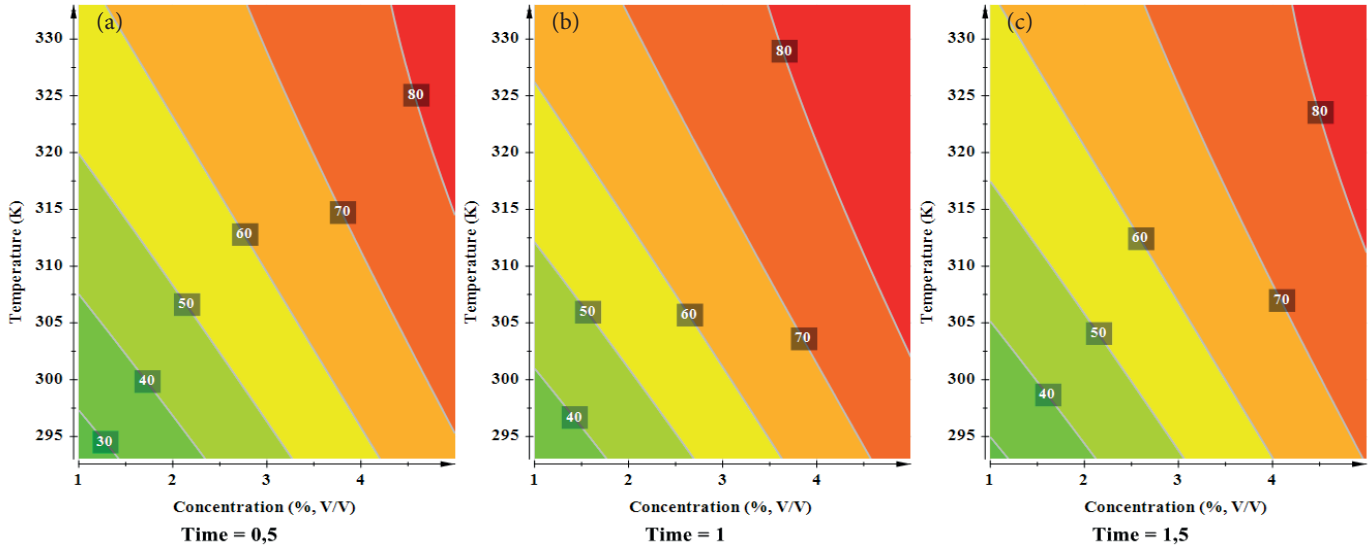


Figure 4: Two-dimensional contour plots of inhibition efficiency (IE%) as a joint function of inhibitor concentration and temperature at fixed immersion times of (a) 0.5 hour, (b) 1.0 hour, and (c) 1.5 hours

Adsorption and Thermodynamic Investigations

The thermodynamic parameters presented in Table 7 offer a comprehensive insight into the corrosion inhibition mechanism of *Ferula communis* L. (Apiaceae) seed essential oil in 0.5 M H_2SO_4. The excellent agreement between the experimental data and both the Arrhenius and transition-state models (R^2 = 0.966–0.999) confirms the robustness of the kinetic analysis and supports the validity of the calculated activation and thermodynamic parameters.

In the inhibitor-free solution, the activation energy (E_{act}) and activation enthalpy (ΔH_{act}) were 41.62 and 39.02 kJ·mol^{-1}, respectively, indicating a comparatively high apparent kinetic barrier for the overall corrosion process, consistent with values reported for uninhibited copper corrosion in sulfuric acid media.[39] Increasing the essential-oil concentration progressively lowered both parameters, reaching 10.94 and 8.34 kJ·mol^{-1}, respectively, at 5% inhibitor. Although a lower is generally associated with a reduced apparent energy barrier, the inhibited systems exhibited higher activation free energies, increasing from 98.26 kJ·mol^{-1} for the blank to 103.59 kJ·mol^{-1} at 5% inhibitor at 313 K. This behaviour is accompanied by a pronounced change in the activation entropy, which became progressively more negative, from −189.25 to −304.32 J·mol^{-1}·K^{-1} as the inhibitor concentration increased. The increasingly negative entropy values are consistent with a more organized activated state at the copper/electrolyte interface, possibly associated with restricted molecular rearrangement in the presence of adsorbed inhibitor constituents.[38] According to , the increasingly negative contribution of more than compensates for the decrease in , thereby producing higher values. These results indicate that the inhibitor substantially modifies the enthalpic and entropic contributions to the overall activation process, with the entropy term making an important contribution to the observed inhibition behaviour.[40]

The difference between and remained constant at approximately 2.60 kJ·mol^{-1} across the investigated systems. This value is essentially equal to at 313 K and is consistent with the theoretical relationship between the Arrhenius and transition-state formulations. This agreement supports the internal consistency of the calculated activation parameters, but it does not provide evidence for a specific elementary reaction or identify a rate-determining step. Accordingly, the present Arrhenius/Eyring analysis based on gravimetric corrosion rates is interpreted in terms of the apparent kinetics of the overall corrosion process rather than being used to assign cathodic hydrogen evolution, or any other elementary step, as the rate-determining reaction.[41] The positive values obtained at 313 K increased progressively with inhibitor concentration, indicating that formation of the activated state becomes less thermodynamically favorable in the presence of increasing amounts of essential oil.

The adsorption behaviour of the essential oil constituents at the copper in 0.5 M H_2SO_4 interface was evaluated by fitting gravimetrically derived surface coverage data collected between 293 and 333 K to four adsorption isotherms: Freundlich, Langmuir, Flory–Huggins, and Frumkin, with the corresponding parameters summarized in Table 7. The suitability of each model was assessed primarily through the coefficient of determination (R^2).[42] All investigated isotherms exhibited satisfactory agreement with the experimental data (R^2 > 0.89), confirming the reproducibility of the adsorption measurements over the entire temperature range. The Langmuir isotherm yielded high correlation coefficients, increasing from 0.970 at 293 K to 0.994 at 333 K. The progressive improvement of the Langmuir fit suggests that adsorption increasingly approaches ideal monolayer behaviour as temperature rises. While the Langmuir model yielded high correlation coefficients, the Frumkin model also provided excellent fits (R^2 = 0.979–0.989), suggesting that lateral interactions between adsorbed species may be relevant. Given the complexity of the essential oil mixture and the limitations of R^2-based model selection, the Langmuir model was retained as a useful phenomenological description rather than as a definitive mechanistic assignment. In contrast, the Flory–Huggins equation produced comparatively lower correlation coefficients (R^2 = 0.891–0.940), suggesting that steric considerations alone do not fully account for the adsorption characteristics of this chemically diverse inhibitor system and that chemical interactions and lateral forces between adsorbates also play a significant role.

A prominent feature of the adsorption parameters is the monotonic increase in the adsorption equilibrium constant with temperature for all investigated models. In the Langmuir formalism, K_{ads} increased from 0.50 at 293 K to 1.54 at 333 K, indicating a progressively stronger affinity of the inhibitor molecules for the copper surface at elevated temperatures. This trend is consistent with the positive adsorption enthalpies obtained from thermodynamic analysis (ΔH_{ads} = +10.80 to +22.65 kJ mol^{-1}), confirming that adsorption is an endothermic and thermally promoted process. [36]

The positive enthalpy values may partly reflect the energetic contribution associated with rearrangement or displacement of interfacial water and ionic species during inhibitor adsorption.[35] The calculated free energies of adsorption remain negative throughout the investigated temperature interval (ΔG_{ads} = −5.10 to −15.20 kJ mol^{-1}), demonstrating the spontaneous character of the adsorption process (Table 8). The relatively moderate magnitude of these values is compatible with a substantial physical contribution to adsorption; however, alone cannot establish a purely physisorptive mechanism, particularly for a chemically complex essential oil containing multiple constituents with potentially different adsorption behaviours.[43] Simultaneously, the large positive entropy changes (ΔS_{ads} = 76.94–105.34 J mol^{-1} K^{-1}) reveal a substantial increase in interfacial disorder upon adsorption. Such behaviour is generally attributed to the release of structured water molecules and adsorbed ionic species from the metal surface during inhibitor uptake.[36] Thus, the thermodynamic parameters describe the overall apparent adsorption process and should not be interpreted as defining the adsorption mechanism of individual essential-oil constituents.[4]

Thermodynamic analysis indicates that adsorption is spontaneous and endothermic, with a substantial entropy contribution to the overall driving force. The relatively moderate negative values of ΔG_{ads} are compatible with a predominantly physical contribution to adsorption; however, they do not exclude localized specific interactions at the Cu/solution interface. In this context, the electron-donating functionalities present in some essential-oil constituents may

Table 7. Thermodynamic activation parameters for the inhibition of copper dissolution by seeds *Ferula communis* L. (Apiaceae) essential oil in 0.5 M H_2SO_4 as a function of inhibitor concentration.

C (%)	$R^2_{(Arrhenius)}$	E_{act} (kJ·mol^{-1})	$R^2_{(Eyring)}$	ΔH_{act} (kJ·mol^{-1})	- ΔS_{act} (J mol^{-1}·K^{-1})	ΔG_{act} (kJ·mol^{-1}) at 313 K
Blank	0.993	41.62	0.991	39.02	189.25	98.26
1	0.984	29.36	0.980	26.76	234.44	100.14
2	0.985	28.60	0.981	26.01	238.22	100.57
3	0.972	29.31	0.966	26.72	237.56	101.08
4	0.977	20.38	0.969	17.78	268.71	101.89
5	0.999	10.94	0.998	8.34	304.32	103.59

Table 8. Comparative evaluation of adsorption isotherm models and thermodynamic parameters for the adsorption of the inhibitor on copper surface at different temperatures

Model	T (K)	R^2	K_{ads}	$-\Delta G_{ads}$ (kJ·mol^{-1})	ΔH_{ads} (kJ·mol^{-1})	ΔS_{ads} (J mol^{-1}·K^{-1})
Langmuir	293	0.970	0.50	8.10	22.65	104.95
	303	0.978	0.714	9.26	22.65	105.31
	313	0.985	0.952	10.32	22.65	105.34
	323	0.991	1.22	11.32	22.65	105.17
	333	0.994	1.54	12.31	22.65	104.98
Freundlich	293	0.965	2.29	12.42	10.80	79.25
	303	0.981	2.70	13.11	10.80	78.98
	313	0.985	3.10	13.73	10.80	78.37
	323	0.982	3.51	14.33	10.80	77.80
	333	0.977	3.85	14.82	10.80	76.94
Flory–Huggins	293	0.891	2.50	11.20	13.60	84.64
	303	0.912	3.15	12.40	13.60	85.81
	313	0.929	3.78	13.50	13.60	86.58
	323	0.940	4.38	14.40	13.60	86.69
	333	0.936	4.91	15.20	13.60	86.49
Frumkin	293	0.979	0.151	5.10	18.12	79.25
	303	0.983	0.195	6.30	18.12	80.59
	313	0.987	0.246	7.40	18.12	81.53
	323	0.989	0.304	8.50	18.12	82.41
	333	0.986	0.369	9.50	18.12	82.94

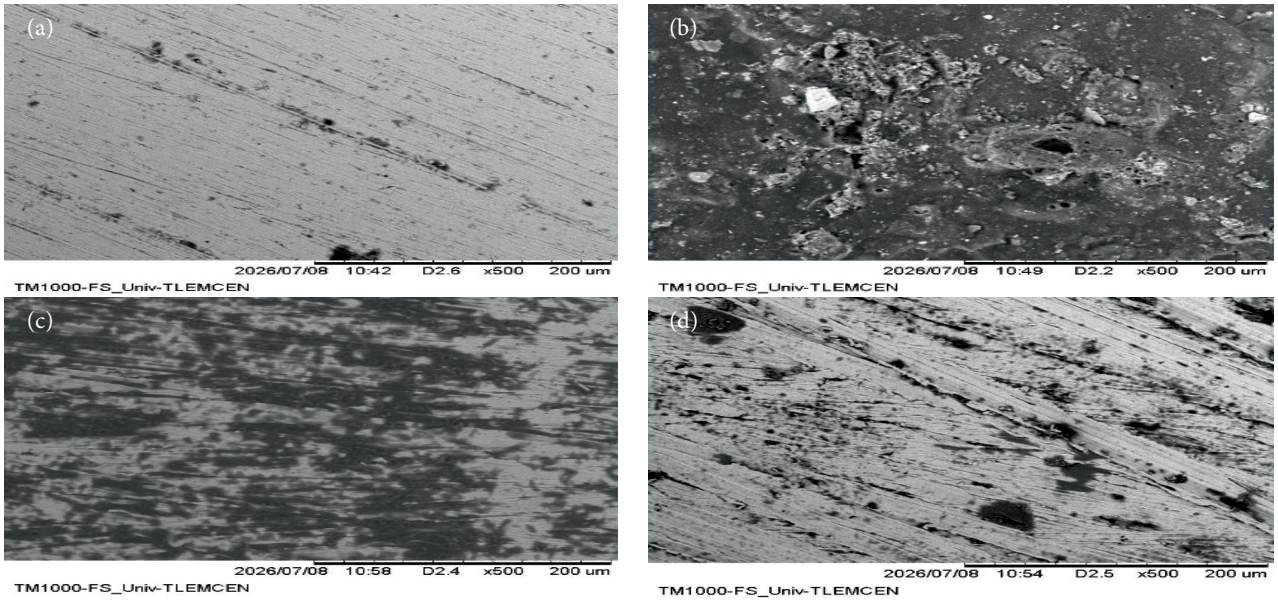


Figure 6: SEM micrographs of the copper surface in 0.5 M H_2SO_4: (a) polished reference, (b) uninhibited control, (c) treated with 1% *Ferula communis* L. seed essential oil at 293 K, and (d) optimized formulation (5% oil, 333 K).

facilitate weak donor–acceptor interactions with surface copper sites, which could contribute to interfacial stabilization. This interpretation remains tentative because such interactions cannot be established directly from gravimetric and thermodynamic measurements alone. The progressive increase in K_{ads} with temperature instead provides evidence for an enhanced apparent affinity of the inhibitor for the copper surface under the investigated conditions.[44,45].

Scanning electron microscopy

The uninhibited copper specimen (Figure 6.b) displays a severely degraded surface characterized by pronounced cavitation, extensive fissuring, and abundant corrosion products, in sharp contrast to the smooth, uniformly polished morphology observed before exposure (Figure 6.a). These features are consistent with the high corrosion rates measured for bare copper in 0.5 M H_2SO_4, in line with morphological degradation reported for copper in the same acidic medium.[46] Upon addition of 1% *Ferula communis* seed essential oil at 293 K (Figure 6.c), surface deterioration is noticeably reduced, with residual polishing marks remaining discernible beneath discontinuous deposits, indicating partial surface coverage by an incompletely developed protective layer, a pattern of intermediate film coverage similarly described for green inhibitors at sub-optimal loading.[44] In contrast, the specimen treated under the optimized conditions (5% inhibitor, 333 K; Figure 6.d) exhibits a remarkably uniform morphology closely

resembling that of the polished reference, with only minimal evidence of localized attack. This pronounced improvement is fully consistent with the inhibition efficiency exceeding 92% predicted by the response surface model and observed experimentally, and parallels findings that elevated temperature can favor denser, more homogeneous film formation rather than film breakdown.[36] The observed surface preservation also agrees with the thermodynamic interpretation of a spontaneous, and predominantly physisorption-controlled adsorption process, in which localized donor–acceptor interactions likely contribute to strengthening the adsorbed film. Overall, the SEM observations are consistent with a barrier-type inhibition mechanism, whereby progressive adsorption of the essential-oil constituents blocks active corrosion sites, while increasing temperature appears to favor the formation of a more homogeneous and protective interfacial layer.

CONCLUSION

This study establishes *Ferula communis* L. seed essential oil as a highly effective, plant-derived inhibitor of copper corrosion in sulfuric acid, through a combined statistical, thermodynamic, and morphological investigation. The response surface model achieved excellent predictive capability (R^2 = 0.996, Q^2 = 0.978), identifying inhibitor concentration as the dominant protective factor, with temperature contributing as a thermally activated promoter. Their strong interaction reveals the shortcomings of one-factor-at-a-time testing and confirms multivariable design as essential for locating true optimum conditions. Immersion time peaked near one hour before progressive film breakdown reduced protection. Thermodynamic analysis indicated spontaneous and endothermic adsorption, with the relatively moderate ΔG_{ads} values being compatible with a predominantly physical contribution. Possible localized donor–acceptor interactions may additionally contribute to interfacial stabilization, although their direct involvement cannot be established from the present measurements alone. Notably, the apparent activation energy fell four-fold, from 41.62 to 10.94 kJ·mol^{-1}, as inhibitor loading increased yet a much larger drop in activation entropy (to −304.32 J mol^{-1}·K^{-1}) raised the activation free energy overall, revealing that protection arises from entropic hindrance of the transition state rather than a simple energy-barrier effect. SEM observations corroborated the proposed adsorption mechanism, showing a compact, continuous film shielding the copper surface. Under the model-optimized conditions (5% inhibitor, 333 K, 1 hour), predicted inhibition efficiency approached 92%, consistent with the high efficiencies measured across the design space. These results establish a transferable framework for engineering next-generation, plant-based inhibitors for industrial acidic processes.

ACKNOWLEDGEMENTS

Authors sincerely thank the research laboratories of Aboubekr Belkaïd University of Tlemcen, Algeria, for their generous support and funding of this work.

AUTHOR CONTRIBUTIONS

D.I.: Design of anticorrosion tests and experiments; D. Y.: Analysis, Writing – Original Draft; S. C.: Conceptualization; B. A.: performed the experiments; EA.M.: Analysis, and Identification; M.A-A.: analysed and interpreted the data; A.M.: analysed data; A. S.: SEM characterization A. T.: Design, Methodology, Writing – Review & Editing, Supervision

DECLARATION OF COMPETING AND FINANCIAL INTERESTS

The authors declare that they have no known competing financial interests or personal relationships that could have appeared to influence the work reported in this paper.

DECLARATION OF GENERATIVE AI AND AI-ASSISTED TECHNOLOGIES

Authors declare that no generative AI or AI-assisted technologies were used in the writing of the manuscript.

ORCID IDS

Ikram Djamai: https://orcid.org/0009-0007-7821-8009
Yazid Datoussaid: https://orcid.org/0000-0002-1696-5320
Chaouki Selles: https://orcid.org/0000-0003-1996-9084
Abbe Benchadli: https://orcid.org/0009-0001-1807-5663
Manal El Ali Ater: https://orcid.org/0000-0003-3540-8412
Alain Muselli: https://orcid.org/0000-0002-0031-1621
Sofiane Amara: https://orcid.org/0000-0001-6033-4617
Tarik Attar: https://orcid.org/0000-0003-2355-1924

REFERENCES

1. Hu P, Cheng P, Wu Y, Guo L, AlObaid AA. Insight into the corrosion inhibition performance of *Capsicum annuum* L. leaf extract as corrosion inhibitor for copper in sulfuric acid medium. J Taiwan Inst Chem Eng. 2024;161:105558. https://doi.org/10.1016/j.jtice.2024.105558.
2. Benzarti Z, Arrousse N, Serra R, Cruz S, Bastos A, Tedim J, Salgueiro R, Cavaleiro A, Carvalho S. Copper corrosion mechanisms, influencing factors, and mitigation strategies for water circuits of heat exchangers: critical review and current advances. Corros Rev. 2025;43(4):429–455. https://doi.org/10.1515/corrrev-2024-0001.
3. Deyab M, Mohsen Q, Bloise E, Lazzoi M, Mele G. Experimental and theoretical evaluations on oleuropein as a natural origin corrosion inhibitor for copper in acidic environment. Sci Rep. 2022;12(1):7579. https://doi.org/10.1038/s41598-022-11598-7.
4. Attar T, Benchadli A. Studying the effectiveness of an expired betamethasone drug in sulfuric acid solutions to examine the corrosive behavior of copper. J. Turk. Chem. Soc. A. 2024;11(1):291–302. https://doi.org/10.18596/jotcsa.1353785.
5. Guo N, Mao X, Liu T, Hui X, Guo Z, Tan B, Shao K, Li X, Zeng Z. Corrosion mechanism of copper in seawater containing bacterial pyomelanin with redox activity. Corros Sci. 2022;204:110407. https://doi.org/10.1016/j.corsci.2022.110407.
6. Zafar F, Bano H, Wahab MF, Corvo F. Mild steel corrosion behavior in a coastal megacity relevant to China Pakistan economic corridor. NPJ Mater Degrad. 2023;7(1):37. https://doi.org/10.1038/s41529-023-00353-6.
7. Shwetha K, Praveen B, Devendra BK. A review on corrosion inhibitors: Types, mechanisms, electrochemical analysis. Results Surf. Interfaces 2024;16:100258. https://doi.org/10.1016/j.rsurfi.2024.100258.
8. Al-Amiery A, Shaker LM. Green and hybrid corrosion inhibitors from adsorption mechanisms to deployable performance. Discov. Electrochem. 2026;3(1):54. https://doi.org/10.1007/s44373-026-00141-2.
9. Qiang Y, Zhang S, Wang L. Understanding the adsorption and anticorrosive mechanism of DNA inhibitor for copper in sulfuric acid. Appl Surf Sci. 2019;492:228–238. https://doi.org/10.1016/j.apsusc.2019.06.190.
10. Medupin RO, Ukoba KO, Yoro KO, Jen T-C. Sustainable approach for corrosion control in mild steel using plant-based inhibitors: A review. Mater. Today Sustain. 2023;22:100373. https://doi.org/10.1016/j.mtsust.2023.100373.
11. Chu T-S, Mai W-J, Li H-Z, Wei B-X, Xu Y-Q, Liao B-K. Insights into the corrosion inhibition performance of plant extracts of different genera in the Asteraceae family for Q235 steel in H_2SO_4. Int J Mol Sci. 2025;26(2):561. https://doi.org/10.3390/ijms26020561.
12. Distefano M, Avola G, Berti S, Riggi E. Germination kinetics of Ferula communis L. seeds, a potentially multipurpose-use wild species. Seeds. 2024;3(2):196–202. https://doi.org/10.3390/seeds3020015.
13. Kavaz D, Faraj RE. Investigation of composition, antioxidant, antimicrobial and cytotoxic characteristics from *Juniperus sabina* and *Ferula communis* extracts. Sci Rep. 2023;13(1):7193. https://doi.org/10.1038/s41598-023-34281-x.
14. Çıvracı S, Yalçın S, Onbaşılar EE. Effects of giant fennel (*Ferula communis* L.) on some performance traits in honey bees during supplementary feeding period. J Apic Res. 2026;65(4):587–594 https://doi.org/10.1080/00218839.2025.2553997.

15. Dahmani K, Galai M, Ech-Chebab A, Al-Zaqri N, Ouakki M, Elgendy A, Ez-Zriouli R, Kim S-C, Touhami ME, Cherkaoui M. Investigating the inhibitory properties of Cupressus sempervirens extract against copper corrosion in 0.5 M H_2SO_4: combining quantum (density functional theory calculation–Monte Carlo simulation) and electrochemical-surface studies. ACS Omega. 2023;8(27):24218–24232. https://doi.org/10.1021/acsomega.3c00589.
16. Beddiar H, Boudiba S, Benahmed M, Hanini K, Tamfu AN, Boudiba L, Soltani H, Laouer H, Akkal S. Evaluation of the Potential of Daucus crinitus Extracts and Their Synthesized ZnO Nanoparticles in Inhibiting the Corrosion of Carbon Steel. J Chem. 2024;2024:1–19. https://doi.org/10.1155/2024/7703829.
17. Fellahi M, Datoussaid Y, Attar T, El Amine Dib M, Benchadli A. Experimental design and statistical modeling for evaluating inhibition efficiency of Daucus crinitus essential oil in corrosion processes. S Afr J Chem. 2025;79:117–124. https://doi.org/10.17159/0379-4350/2025/v79a12.
18. Europe Co. *European Pharmacopoeia*. 3rd ed. Strasbourg: Council of Europe; 1997.
19. El Ali M, Tintaru A, Muselli A. New findings from the volatiles of the Corsican liverwort Porella arboris-vitae: an evaluation of their allelopathic effect. J Agric Food Chem. 2025;73(9):5102–5115. https://doi.org/10.1021/acs.jafc.4c10963.
20. Kumari P, Lavanya M. Optimization Strategies for Corrosion Management in Industries with Artificial Neural Network and Response Surface Technology: A Comprehensive Review. J Bio Tribocorros. 2024;10(3):59. https://doi.org/10.1007/s40735-024-00863-z.
21. Benabdallah M, Touati Y, Datoussaid Y, Attar T, Benchadli A, Yousfi Y, Choukchou-Braham E, Choukchou-Braham N. Green synthesis of rhodanine-derived inhibitors for carbon steel corrosion protection: DFT, thermodynamic, and surface analysis. Prot Met Phys Chem Surf. 2025;61(5):1201–1212. https://doi.org/10.1134/S2070205125700820.
22. Kheroubi B, Datoussaid Y, Benchadli A, Attar T. Optimization and thermodynamic characteristics of copper corrosion inhibition by expired Toplex syrup in sulfuric acid. J. Chem. Technol. Metall. 2026;61(3):447–458. https://doi.org/10.59957/jctm.v61.i3.2026.7.
23. Chen L, Lu D, Zhang Y. Organic compounds as corrosion inhibitors for carbon steel in HCl solution: A comprehensive review. Materials (Basel). 2022;15(6):2023. https://doi.org/10.3390/ma15062023.
24. Aldahiri RH, Hussein MA, Al-Bukhari SM, Alamry KA, Khan A, Aslam R. Synergistic effect of Canarium strictum leaves extract and KI on the corrosion protection of mild steel in 15% HCl solution. Sci Rep. 2025;15(1):3576. https://doi.org/10.1038/s41598-025-87482-x.
25. Vaszilcsin CG, Putz MV, Kellenberger A, Dan ML. On the evaluation of metal-corrosion inhibitor interactions by adsorption isotherms. J Mol Struct. 2023;1286:135643. https://doi.org/10.1016/j.molstruc.2023.135643.
26. Benhadria N, Attar T, Benchadli A, Choukchou-Braham E. The study of expired pharmaceutical drug as corrosion inhibitor for carbon steel in acidic media using the design of experiment. Rev Roum Chim. 2024;68(10-12):515–525. https://doi.org/10.33224/rrch.2023.68.10-12.03.
27. Beniken M, Driouch M, Sfaira M, Hammouti B, Ebn Touhami M, Mohsin M. Kinetic–thermodynamic properties of a polyacrylamide on corrosion inhibition for C-steel in 1.0 M HCl medium: Part 2. J Bio Tribocorros. 2018;4(3):34. https://doi.org/10.1007/s40735-018-0152-1.
28. Mohamad Alwi MA, Ahmad MN, Misnon II, Pauzi H, Normaya E. Gravimetric and electrochemical statistical optimizations for improving copper corrosion resistance in hydrochloric acid using thiosemicarbazone-linked 3-acetylpyridine. RSC Adv. 2022;12(43):27793–27808. https://doi.org/10.1039/D2RA05192C.
29. Belkhodja A, Choukchou-Braham E, Benkhaled A, Guendouz S, Attar T. Study of the Adsorption of a Textile Dye by Alginate-Bentonite Beads: CCD-RSM Design Conception. J Macromol Sci Part B Phys. 2026;65(4):567–589. https://doi.org/10.1080/00222348.2024.2437854.
30. Attar T, Benchadli A, Choukchou Braham E, Benkhaled A. Iodine–β-cyclodextrin: an effective corrosion inhibitor for carbon steel in sulfuric acid solution—experimental design and investigating thermodynamic parameters. J. Turk. Chem. Soc. A. 2024;11(1):161–170. https://doi.org/10.18596/jotcsa.1346065.
31. Okpanachi CB, Ameh EM, Onoyima CC, Ekwoba L, Larayetan R, Abalaka E, Ejukwa E. Factor interactions governing aluminium corrosion inhibition by Sida acuta leaf extract: response surface methodology and gravimetric study. UMYU Sci. 2026;5(2):77–90. https://doi.org/10.56919/usci.2652.008.
32. Jasim ZI, Rashid KH, Al-Azawi KF, Khadom AA. Optimization of the corrosion inhibition performance of novel oxadiazole thione-based Schiff base for mild steel in HCl media using Doehlert experimental design. Inorg Chem Commun. 2024;160:111911. https://doi.org/10.1016/j.inoche.2023.111911.
33. Ahmadi S, Khormali A. Optimization of the corrosion inhibition performance of 2-mercaptobenzothiazole for carbon steel in HCl media using response surface methodology. Fuel. 2024;357:129783. https://doi.org/10.1016/j.fuel.2023.129783.
34. Jomy J, Prabhu D. Custom design approach of design of experiment as a tool for the optimisation of parameters for corrosion inhibition study of (+)-arabinogalactan on AISI 5140 steel. Corros Eng Sci Technol. 2025;60(1):62–76. https://doi.org/10.1177/1478422X241272083.
35. Suprapto S, Ardiansyah H, Sugiarso D, Madurani KA, Manuhara YSW, Syamsuardi S. Statistical optimization and electrochemical analysis of gambir extract as a corrosion inhibitor for SS-316 in hydrochloric acid. Case Stud Chem Environ Eng. 2024;10:100891. https://doi.org/10.1016/j.cscee.2024.100891.
36. Mzioud K, Habsaoui A, Rached S, Ech-chihbi E, Ouakki M, Salghi R, Touhami ME. Experimental investigation and theoretical modeling of copper corrosion inhibition by Urginea maritima essential oil. Mater. Today Sustain. 2024;27:100906. https://doi.org/10.1016/j.mtsust.2024.100906.
37. Guo X, Zhang X, Ma L, Li Y, Le J, Fu Z, Lu L, Zhang D. Understanding the adsorption of imidazole corrosion inhibitor at the copper/water interface by ab initio molecular dynamics. Corros Sci. 2024;236:112237. https://doi.org/10.1016/j.corsci.2024.112237.
38. Garg V, Zanna S, Seyeux A, Wiame F, Maurice V, Marcus P. Interfacial bonding and corrosion inhibition of 2-mercaptobenzimidazole organic films formed on copper surfaces under electrochemical control in acidic chloride solution. Electrochim Acta. 2024;484:144114. https://doi.org/10.1016/j.electacta.2024.144114.
39. Attar T, Choukchou-Braham E, Dali Youcef B, Benchadli A, Mellal T, Benabdelkader I. Application of polyvinylpyrrolidone-iodine complex as a corrosion inhibitor for carbon steel using experimental design method. Alg. J. Eng. Technol. 2022;6:14–18. https://doi.org/10.57056/ajet.v6i1.68.
40. Mzioud K, Habsaoui A, Ouakki M, Galai M, El Fartah S, Ebn Touhami M. Inhibition of copper corrosion by the essential oil of Allium sativum in 0.5 M H_2SO_4 solutions. SN Appl Sci. 2020;2(9):1611. https://doi.org/10.1007/s42452-020-03393-8.
41. Attar T, Benchadli A, Choukchou-Braham E. Inhibition of corrosion of copper by polyvinylpyrrolidone-iodine in sulfuric acid medium. Alg. J. Mater. Chem. 2022;5:1–8. https://doi.org/10.5281/zenodo.5855835.
42. Motlagh ZJ, Karimi M, Bozorg M, Rahimifard M, Mahdavi M. Zataria multiflora essential oil as a green corrosion inhibitor for copper in HCl electrolyte. Mater Today Commun. 2026;52:115067. https://doi.org/10.1016/j.mtcomm.2026.115067.
43. Datoussaid Y, Missoum H, Attar T, Messaoudi B, Benchadli A, Choukchou-Braham E, Choukchou-Braham N, Ziani-Cherif C. Experimental and theoretical studies of aminothiophene derivatives inhibitors on carbon steel corrosion in perchloric acid medium. Rev Roum Chim. 2024;69(3-4):139–148. https://doi.org/10.33224/rrch.2024.69.3-4.04.
44. Rached S, Mzioud K, Habsaoui A, Galai M, Dahmani K, Ouakki M, Fartah S. Inhibition of copper corrosion in sulfuric acid by Mentha pulegium L. Port Electrochem Acta. 2024;42(2):137–153. https://doi.org/10.4152/pea.2024420205.
45. Deyab MA, Al-Ghamdi JM, Abdeen MM, Elfattah MA, Galhoum A, El-Shamy OAA, El-Sayed IE. Chemical, electrochemical, and quantum investigation into the use of an organophosphorus derivative to inhibit copper corrosion in acidic environments. Sci Rep. 2024;14(1):11395. https://doi.org/10.1038/s41598-024-60614-5.
46. Adel O, Mohamed ME, Khamis E. Thermodynamic, electrochemical and surface characterization of copper corrosion inhibition in acidic solution using rice straw extract. Sci Rep. 2025;15(1):27753. https://doi.org/10.1038/s41598-025-12482-w.